PHYSICAL REVIEW B

CONDENSED MATTER

THIRD SERIES, VOLUME 42, NUMBER 17 15 DECEMBER 1990-I

Analysis of experimental extended x-ray-absorption fine-structure (EXAFS) data using calculated curved-wave, multiple-scattering EXAFS spectra

Jose Mustre,* Yizhak Yacoby, Edward A. Stern,† and John J. Rehr†

Racah Institute of Physics, Hebrew University of Jerusalem, 91 904 Jerusalem, Israel

(Received 17 July 1989; revised manuscript received 27 June 1990)

We present an EXAFS analysis method that is accurate and generally applicable and can be implemented on a fast microcomputer within a reasonable amount of computation time. The analysis is based on the comparison between a calculated EXAFS spectrum of a parametrized model with the experimental spectrum and the refinement of the model parameters. The calculated EXAFS spectrum is evaluated taking into account the curved-wave nature of the photoelectron and multiple scattering up to and including third-order collinear scattering. Such an expansion treats accurately all multiple-scattering contributions that contribute to the Fourier transform of the EXAFS spectrum up to the fourth-neighbor distance. The comparison between theory and experiment is thus limited to this distance. In this calculation we schematically express the contributions of the various scattering configurations η in the form $\chi_0^\eta = F_\eta(k)\sin[kL_\eta + \Theta_\eta(k)]$ and expand to lowest order the amplitude F_η and the phase Θ_η functions in terms of all structural and potential parameters. This expansion is quite accurate and significantly speeds up the computation. We discuss a set of parameters which seems to account for the limitations in the employed theory, providing a very good fit between theory and experiment. The analysis method and the parameters have been implemented successfully on a number of systems. We present here the analysis of the copper EXAFS spectrum. The experimental data contain 20 independent experimental points; yet we obtain a very good fit with only six parameters. The results also show the importance of both double and triple collinear scattering as well as the importance of noncollinear double scattering.

I. INTRODUCTION

Since its introduction as a structure analytical tool in 1971,[1] extended x-ray-absorption fine structure (EXAFS) has contributed many interesting results on the microscopic structure of condensed-matter systems. Many of these results could not have been obtained otherwise. An important element in obtaining structural information is a reliable method for analyzing the experimental results.

The conventional EXAFS data analysis method has two important advantages. First, it is simple and it is very inexpensive in terms of the computer time used yet it provides useful structural information. Second, it provides structural information without the need for an *a priori* structural model. It has, however, several disadvantages. It is based on the plane-wave EXAFS theory, which is not adequate at low energies. The use of a standard for comparison helps but does not solve the problem completely. In addition, it does not take into account multiple scattering, which plays an important role at distances beyond the first shell.

A great deal of progress has been achieved in recent years in the theory of EXAFS. Formulations that take into account the spherical-wave nature of the photoelectron for both single and double scattering were introduced by Schaich,[2] Lee and Pendry,[3] and Ashley and Doniach[4] based on the multiple-scattering expansion. A related method based on the full solution of the multiple-scattering problem in a cluster has been developed by Durham *et al.*[5] and applied, for example, by Gurman and Pettifer[6] to the case of As_2O_3. The main problem with these formulations is that they are quite involved computationally since they take into account multiple-scattering events to all orders within a given shell, and thus their application is not yet practical in routine experimental analysis. Theoretical and experimental work[3,7,8] showed that multiple-scattering effects, even near the edge, are weak enough, so that an expansion in the order of the multiple scattering will be useful. Vvedensky *et al.*[9] extended the previous work of Pendry and co-workers so as to isolate the various multiple-

scattering contributions.

A simpler formulation that took spherical-wave effects into account exactly in single scattering was introduced by Müller and Schaich.[10] The concept of an effective scattering amplitude analogous to the plane-wave scattering amplitude was introduced by Rehr *et al.*[11] and was extended to treat multiple-scattering events. This formulation is fast enough to be used routinely in the experimental analysis of the first few shells. This formulation implemented for the case of powder sample measurements was compared with band-structure calculations in the case of Cu.[12]

Independently, Gurman *et al.*[13] introduced a fast exact formulation for single and multiple scattering that includes up to triple-scattering events, applicable to powder sample measurements. They showed the applicability of this formulation analyzing the first two shells of $Co(CO)_4$. In their method they used the Mattheiss prescription[14] for the construction of the muffin-tin potential and an $X\alpha$ approximation for the exchange potential. More recently, Gurman[15] formulated a multiple-scattering approach based on the small-atom approximation that speeds up the multiple-scattering calculation. Our programs are based on the formulations of both Rehr *et al.*[12] and Gurman *et al.*[13]

These theoretical developments facilitated a new kind of EXAFS data analysis. Harris, Hukins, and Hasnain,[16] at Daresbury Laboratory, developed an analysis system that operates in the following way. A structural model with several structural parameters is assumed. The theoretical EXAFS spectrum for this structure is calculated taking into account the spherical nature of the wave function as well as multiple-scattering contributions. The atomic potentials involved in the calculation are also parametrized. The calculated spectrum is compared to the experimental results and the parameters are varied so as to minimize the sum of squares of the differences between the two. One usually uses a reference material with a known structure in order to obtain information on the relevant atomic potential parameters.

The main difficulty in this scheme is that it requires a lot of computer time even in moderately fast computers such as the Digital Equipment Corporation VAX. The reason is that it is necessary to calculate the EXAFS spectrum a large number of times in the process of fitting the theory with experiment. Our method speeds up this process by more than an order of magnitude as discussed below Eq. (1).

The theoretical approach adopted here has a number of other advantages over other methods for calculation of XAFS. Our method is based on the general multiple-scattering theory of XAFS, and focuses on those contributions to XAFS from relatively short distance single- and multiple-scattering paths. In practice we include multiple scattering up to third order, which corresponds to distances typically up to fourth neighbors. There are only a small number of such terms, and each of them is treated either exactly or to high accuracy by current curved-wave scattering theory.

The Daresbury EXCURVE program[13,17] also includes multiple scattering only up to triple-scattering paths but it does not separate the various contributions like our procedure does. The molecular potential in our procedure is treated crudely by ground-state standards, but is probably adequate for EXAFS studies. Like EXCURVE, our program also uses an $X\alpha$ exchange potential with an adjustable parameter to compensate for the lack of energy dependence in the exchange. In the future these drawbacks can be remedied by incorporating a more-accurate overlapped-atom potential and a modern energy-dependent exchange-correlation potential. However, these refinements will not change the overall scope of this work.

In a Fourier transform of the XAFS spectra, our multiple-scattering expansion is able to completely represent the data up to fourth-nearest-neighbor distances. The advantage of separating out each multiple-scattering path is that one can determine different parameters for each path when appropriate. For example, the first neighbor is expected to have a different Debye-Waller factor from more-distant neighbors, and this can be incorporated in our procedure. Similarly, for multiple-scattering paths a different Debye-Waller factor is likely to be important. We also allow the mean-free-path parameter to vary with path to compensate for the lack of an energy-dependent imaginary self-energy in the theory. This separation of paths also makes it possible to determine which paths contribute most significantly to the XAFS data for a given structural distortion, so that one can obtain a qualitative interpretation of various features in the data. This permits one to "trouble shoot" and isolate particular paths that may have peculiar contributions. By contrast, other methods (e.g., band structure and cluster) that rely on exact diagonalizations implicitly include multiple-scattering paths to all orders, with a crude approximation for Debye-Waller and inelastic effects. However, as the computation time increases quite rapidly with energy, such methods are essentially limited to the near-edge region.

In our procedure, we express the EXAFS spectrum as a sum of different multiple-scattering contributions. Each such contribution can be expressed in the form

$$\chi_\eta(k)=\chi_0^\eta(k)\exp(-L_\eta/\lambda_\eta-2k^2\sigma_\eta^2)$$

and

$$\chi_0^\eta=F_\eta(k)\sin[kL_\eta+\Theta_\eta(k)]\ . \tag{1}$$

Here η represents different single- or multiple-scattering paths, and L_η is the total path length. F and Θ are the amplitude and phase which depend on k, on the specifics of the scattering path involved, and on the atomic potential parameters.

To overcome the need to recalculate the entire EXAFS spectrum every time the fitting routine requires it, we would like to expand χ in terms of the various structural and atomic parameters. However, even if the range of structural variation is small (of the order of 10% of the distances), Eq. (1) cannot be linearly expanded in the structural parameters because of the large kL_η term. On the other hand, for $k>3$ Å, F_η and Θ_η are slowly varying functions of the structural and potential parameters and

can therefore be linearly expanded. The validity of this linear expansion was checked and the deviation from linearity in the range that the parameters may vary was found to be negligible. The one exception is double and triple scattering, where two atoms are collinear with the center atom, or almost so (focusing or shadowing). In that case, the expansion is second order in the angle deviation from collinearity. Thus we create a table of all the relevant amplitudes and phases and their first derivatives with respect to all the interatomic distances, angles, and potential parameters. This table can then be used to calculate F_η and Θ_η for various parameter values. This eliminates the need to calculate the EXAFS spectra every time it is needed in the process of refining the parameters.

As discussed below, the theoretical calculation of EXAFS still suffers from a number of limitations. The parameters we introduce to correct for these flaws are different from the ones used by Harris *et al.*[16] These parameters will be discussed in some detail in this paper.

The aspect that permits a tractable multiple-scattering expansion is the connection between L_η and the order of the multiple scattering. When the $\chi_\eta(k)$ of a particular scattering path is Fourier transformed by e^{i2kr} into r space, it contributes at an approximate $L_\eta/2$ shifted by ~ 0.5 Å due to the k dependence of Θ_η. If one limits the r-space region fit to be $r < R_0$, then the maximum order to the multiple scattering that can contribute to the results is $n \approx (2R_0/d - 1)$, where d is the nearest-neighbor distance between atoms in the material.[18] For example, for the first neighbor where $r = d$, $n = 1$, only single scattering contributes. In the case discussed in this paper, we fit up to a distance R_0, where it is necessary to include scattering only up to third order.

In the next section, we discuss the method we used for calculating the EXAFS contributions, namely, the calculation of F_η and Θ_η. In Sec. III we discuss briefly the structure of the fit programs. We also discuss the limitations of the theory and the parameters used in order to correct for them. In Sec. IV we present the analysis of the EXAFS of copper as an example. A summary of the analysis method will be presented in Sec. V.

II. CALCULATION OF THE EXAFS SPECTRUM

The calculation of the EXAFS spectra involves three main steps. First we calculate the muffin-tin potential using the atomic code written by Descleaux.[19] Then we use this muffin-tin potential to calculate the scattering phase shifts. Finally, the phase shifts are used in the evaluation of the EXAFS absorption formulas, which take into account the spherical-wave nature of the final photoelectron state. The EXAFS formulas used are applicable for measurements carried out in polycrystalline or amorphous samples, where one can consider an average of the polarization direction of the photon beam.

In the calculation of the muffin-tin potential, we take as a starting point a self-consistent solution of the Dirac equation for the atom or ion of interest. In the case of the absorbing atom, we include a hole in the core state. This choice of configuration corresponds to a final state in between the screened and unscreened states described by Lee and Beni.[20] The exchange-correlation potential in this atomic calculation is approximated by the $X\alpha$ potential, a form similar to that used in band-structure calculations of ground-state properties. The charge density obtained in this way is truncated at the Wigner-Seitz radius as a uniform charge density. Given this charge density, a muffin-tin potential is obtained. For the case of Cu, there are only small differences in the calculated EXAFS spectrum using this prescription[21] to calculate the muffin-tin potential instead of the more-exact self-consistent potential or a potential built using Mattheiss's[14] prescription. However, in the case of molecules or solids containing atoms of low coordination numbers, the use of a self-consistent potential is important in order to obtain a phase factor in EXAFS that allows an accurate estimation of interatomic distances.[22] The use of the $X\alpha$ potential is also known to introduce errors in the phase factor of calculated EXAFS.[20] In order to eliminate these errors, it is necessary to use a complex, energy-dependent potential as discussed by Lee and Beni[20] and Teo and Lee.[23] We are currently modifying our set of programs to include such a potential.

The phase shifts for each atom in the system are evaluated using the calculated muffin-tin potential and a zero potential in the interstitial region. Specifically, we integrate the Dirac equation up to the muffin-tin radius and match this solution and its derivative to free spherical waves at the muffin-tin radius. At this stage of the calculation of the phase shifts, we ignore relativistic corrections due to the spin of the electron, using the same potential for all electrons independent of their spins.

Single-scattering contributions are calculated exactly within a single-particle curved-wave theory using the formulation of Rehr *et al.*,[8]

$$\chi_0^{(1)}(E) = -\sum_{\mathbf{R}_i} \frac{|\tilde{f}(\pi,R_i)|}{kR_i^2} \sin(2kR_i + 2\delta_l^c + \Phi) \ . \qquad (2)$$

$\mathbf{R}_i$ denotes the vector from the central atom to atom i, $E = \hbar\omega - E_0$ is the energy of the photoelectron, $\hbar\omega$ is the photon energy, E_0 is the energy of the core level below the Fermi energy, $k = \sqrt{2mE}/\hbar$ is the photoelectron wave number, δ_l^c is the $l = 1$ central atom phase shift, and $\tilde{f}(\pi,R_i)$ is a distance-dependent effective scattering amplitude given by

$$\tilde{f}(\pi,R_i) = |\tilde{f}(\pi,R_i)|e^{i\Phi} = (1/k)\sum_l (-1)^l(2l+1)t_l^i \left[\frac{(l+1)c_{l+1}^2(kR_i) + lc_{l-1}^2(kR_i)}{2l+1} \right] , \qquad (3)$$

where c_l is the polynomial part of the spherical Hankel functions, i.e., $h_l(x) \equiv i^{-l}(e^{ix}/x)c_l(x)$, and t_l^i denotes the l component in an angular-momentum basis of the scattering matrix of atom i. Equation (1) has the same form as the plane-wave EXAFS formula, however, the ordinary backscattering amplitude $\tilde{f}(\pi)=(1/k)\sum_l(-1)^l(2l+1)t_l$ has been replaced by the effective scattering amplitude $\tilde{f}(\pi,R)$, which takes into account the spherical-wave effects. The particular form of $\tilde{f}(\pi,R)$ that we use is applicable to measurements in polycrystalline samples or amorphous materials, where the polarization direction of the photon beam is averaged over all crystalline axes, but cannot be used for measurements in single-crystal samples done with polarized x rays. As discussed in Sec. I, inelastic effects are introduced by the mean free path λ and lattice vibrations through the use of a Debye-Waller factor $\exp(-2k^2\sigma^2)$. These are used as parameters to be determined by the fit.

As in the single-scattering case, double scattering contributions are calculated exactly within a single-particle framework. In this case we use expressions obtained by Gurman *et al.*[13]

$$\chi_0^{(2)}(E)=\frac{2}{2l_f+1}\mathrm{Re}\sum_{m_f} Z_{l_f m_f, l_f m_f} , \tag{4}$$

where l_f and m_f denote the orbital and magnetic quantum number of the final photoelectron state, respectively, and

$$\sum_m Z^{(2)}_{lm,lm}=e^{2i\delta_l^c}\sum_{l_1,l_2,\lambda_1,\lambda_2,\lambda_3} h_{\lambda_1}(kR_1)h_{\lambda_2}(k|\mathbf{R}_2-\mathbf{R}_1|)h_{\lambda_3}(kR_2)t_{l_l}^1 t_{l_2}^2(2l+1)(2l_1+1)(2l_2+1)(2\lambda_1+1)(2\lambda_2+1)(2\lambda_3+1)$$
$$\times\begin{pmatrix} l & \lambda_1 & l_1 \\ 0 & 0 & 0\end{pmatrix}\begin{pmatrix} l_1 & \lambda_2 & l_2 \\ 0 & 0 & 0\end{pmatrix}\begin{pmatrix} l & \lambda_3 & l_2 \\ 0 & 0 & 0\end{pmatrix}W(\lambda_1 l_1 \lambda_3 l_2; l\lambda_2)$$
$$\times(-1)^{\lambda_3+l_1}\sum_\mu\left(\frac{4\pi}{2\lambda_2+1}\right)^{1/2}Y_{\lambda_2,-\mu}(\mathbf{R}_2-\mathbf{R}_1)\left(\frac{4\pi}{2\lambda_3+1}\right)^{1/2}Y_{\lambda_3\mu}(\mathbf{R}_2)\begin{pmatrix}\lambda_2 & \lambda_1 & \lambda_3 \\ \mu & 0 & -\mu\end{pmatrix} . \tag{5}$$

Here, $Y_{lm}(\mathbf{R})$ is a spherical harmonic,[23] $\begin{pmatrix} l_1 & l_2 & l_3 \\ 0 & 0 & 0\end{pmatrix}$ denotes a Clebsh-Gordan coefficient as defined by Brink and Satchler,[24] $W(l_1,l_2,l_3,l_4;l,l')$ is a $6j$ symbol as defined by Brink and Satchler.[23] The sums over l_i and λ_i are restricted by the condition that both the Clebsch-Gordan coefficients and $6j$ symbols do not vanish.

Even with the use of the fast formulation of Gurman *et al.*[13] the calculation of the double-scattering contribution was already the main computational bottleneck in our full EXAFS calculation. Thus, an exact calculation of the triple-scattering contributions was considered impractical under the given circumstances. Instead, we used the asymptotic theory for multiple scattering developed by Rehr *et al.*[11] We started with the expression for EXAFS in terms of the single-particle free propagator:

$$\chi_0^{(3)}(E)=-\mathrm{Im}\left[e^{2i\delta_l^c}\frac{2}{2l_f+1}\right.$$
$$\times\sum_{m_f,L_1,L_2,L_3} G_{L_f L_1}(\mathbf{R}_1)t_{l_1}^1 G_{L_1 L_2}(\mathbf{R}_2-\mathbf{R}_1)$$
$$\times t_{l_2}^2 G_{L_2 L_3}(\mathbf{R}_3-\mathbf{R}_2)$$
$$\left.\times t_{l_3}^3 G_{L_3 L_f}(-\mathbf{R}_3)\right] , \tag{6}$$

where $L\equiv(l,m)$, $G_{LL'}(\mathbf{R}_i)$ denotes the free-particle propagator in an angular-momentum basis $\langle \mathbf{r}|L,\mathbf{R}\rangle = (-i)^l j_l(k|\mathbf{r}-\mathbf{R})$, and $j_l(x)$ is a spherical Bessel function. The propagator is approximated by

$$G_{LL'}(\mathbf{R})=4\pi Y_L(\hat{R})Y_{L'}(\hat{R})\frac{e^{i\rho}}{\rho}g_{ll'}^{(0)}(\rho) , \tag{7}$$

with $\rho=kR$, and

$$g_{ll'}^{(0)}\approx\left[1+\frac{\mathcal{L}^2+(\mathcal{L}')^2}{2\rho^2}\right]e^{i[\mathcal{L}^2+(\mathcal{L}')^2]/2\rho}J_0(\mathcal{L}^2(\mathcal{L}')^2/\rho^2) . \tag{8}$$

Here, $\mathcal{L}^2\equiv l(l+1)$ and J_0 is the Bessel function of order 0. The accuracy of this approximation has been documented by Rehr *et al.*[11] For scattering paths along a straight line it is found to be exact, while for angles up to 20° it produces errors of less than 10% in the amplitude and 0.15 rad in the phase when compared with the exact calculation. This point is important since, as pointed out,[8-11] one expects shadowing and low-angle contributions to be important contributions in the EXAFS spectrum arising from shells above the second one. As was the case in the single-scattering contribution [Eq. (2)], Eqs. (4) and (6) are valid only for measurements in polycrystalline or amorphous samples. The amplitude and phase functions, as defined in Eq. (1), can be obtained for the double- and triple-scattering contributions by dividing the corresponding complex expressions for χ_0 [Eqs. (4) and (6)] by $\exp(ikL_\eta)$. The amplitude and the phase functions are the k-dependent absolute value and phase of this ratio.

III. THE FITTING OF THEORY AND EXPERIMENT

The process of analyzing the data is as follows. We first define an idealized structure, one which we believe is

close enough to the real structure in order to be able to use the linear expansion of the amplitude and phase functions. For this structure we calculate F_η and Θ_η as a function of k, as well as their first derivatives with respect to all atomic parameters that we may want to vary, and with respect to the structural parameters of the scattering configurations involved. The scattering-configuration structural parameters are the distances and bond angles among the atoms involved. The validity of the linear expansion of F_η and Θ_η with respect to the structural parameters was checked by directly calculating the functions for three values of each parameter. The parameter values were chosen so that they would differ from each other by quantities that are characteristic of the variations that are likely to be found in the refinement process. Namely, 0.1 Å for the distances and 0.05 rad for the bond angles. The deviations from linearity were found to be about 1% in the amplitudes and about 0.05 rad in the phase. These deviations are completely negligible.

The amplitude and phase functions and their derivatives are used by the fitting routine and are sufficient in order to calculate the EXAFS spectrum, given the atomic parameters and the scattering-configuration structural parameters of all the configurations involved. We now define a set of parametrized distortions, which we assume can transform our idealized structure into the correct structure of the system under investigation. Such distortions may include, for example, a change in one or more of the unit-cell dimensions, a displacement of a certain atom or atoms in a prespecified direction, etc. Each distortion may effect the structural parameters of one or more of the scattering configurations. We therefore supply the fitting routine with a second table. This table contains the derivatives of the scattering-configuration structural parameters of all the scattering configurations (interatomic distances and bond angles), with respect to all the structural distortion parameters. This is done by a general program for any structural model with any set of structural distortion parameters.

The fitting procedure is now quite simple. The two tables are used in a subroutine to calculate the EXAFS spectrum for any set of structural distortions and atomic parameters. This subroutine is part of the least-squares-fit program, which refines the parameters. Notice that changing the model (for example displacing the probe atom in the [100] direction instead of the [111] direction) requires a change in the second table but not in the first. Since the main computer-time investment needed is for calculating the first table, such a change requires relatively little time. Once the table of the F_η and Θ_η and their first derivatives have been evaluated, the time required to fit theory and experiment is about 1 h on a fast microcomputer.

The fit itself can be performed in several ways. It is possible to fit the EXAFS spectrum itself, its Fourier transform, or both. In principle one would obtain exactly the same results if the fit is performed to the original spectrum or to its Fourier transform (but not to the absolute value of the transform). To obtain a meaningful fit, it is necessary to limit the fitting range in both **k** and **r** spaces for the following reasons. At small **k** values the theory is quite unreliable. At large **k**'s the signal-to-noise ratio becomes poor. In the Fourier-transformed spectra the data at small distances are very unreliable because they depend on the background subtraction. In addition, since we limit our theory to a given total path length (to avoid multiple scattering of higher order than collinear third order), we must also limit the fitting range in **r** space to half this distance. The two ranges in **k** and **r** spaces actually define the number of truly independent experimental points:[25]

$$N_{\rm exp}=2\,\Delta k\,\Delta r/\pi\ . \tag{9}$$

Thus, we adopted the following fit procedure. We define the range in **k** in which the results are useful. The data in this range are Fourier transformed and the fit is performed over the useful range in **r** space only.

As pointed out in Sec. II, the presently available theory has a number of flaws. In order to obtain a good fit with experiment, we introduce a number of parameters that are refined together with the structural parameters. The $X\alpha$ potential that we use is real. Consequently, the loss in the phase of the photoelectron is not accounted for. We therefore introduce the mean free path as a parameter in Eq. (1). The energy dependence of the exchange correlation potential is neglected. This leads to a **k**-independent error in the phase, which is corrected by assuming a **k**-independent phase correction as a parameter. The differences between the zeros of the ionic potential functions and the Fermi level are not known. In addition, the scattering potential of each ion depends on its precise ionic state, which in turn depends on the rest of the system. Even a small error of 0.1 electrons in the ionic state leads to large errors in the phase. It turns out that the error introduced by both uncertainties is a phase change that is approximately inversely proportional to **k**. The proportionality constants for each of the different ions are therefore used as fit parameters.

The data-analysis system and the parameters we introduce to account for the flaws in the theory have been found to work very well in all six systems we have analyzed so far. We shall present in the next section one example. The analysis of the other systems will be published elsewhere.

IV. ANALYSIS OF THE COPPER EXAFS DATA

We chose to test our data-analysis method on the EXAFS of copper. The test had two purposes. First, to see if in a system with a known structure the theoretical EXAFS results can be made to agree with the experiment. A successful fit would indicate that the parameters we chose in Sec. III are indeed sufficient in order to correct for the flaws in the theory. Second, we wanted to investigate the importance of multiple-scattering contributions, namely the relative magnitudes of the single-, the noncollinear double-, and the collinear double- and triple-scattering contributions. The EXAFS spectrum of copper after removing the background is shown in Fig. 1. The data were measured using our laboratory EXAFS system in Jerusalem.[26] The parameters which were used in the fitting procedure were as follows.

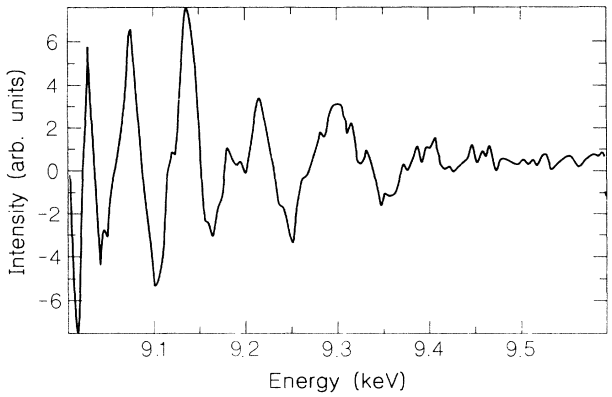

FIG. 1. The EXAFS spectrum of copper as a function of energy after removing the background.

(a) The atomic potential parameters, the muffin-tin radius r_{MT}, and the charge density exponent α were taken from tables and are equal to 1.48 Å and 0.707, respectively. Varying these parameters even over a relatively wide range did not improve the fit significantly. Thus in our final analysis these parameters were not allowed to vary.

(b) The many-body correction parameter[27] S^2 was also taken from tables. For a given number of atoms in a shell the parameters that affect the EXAFS intensity are S^2, the mean free path λ, and the Debye-Waller factor $\exp(-2k^2\sigma^2)$. It turns out that if the **k** range is limited, a small change of one of these parameters can be easily compensated for by the others, so that the fit quality is essentially undamaged. We therefore took the value of S^2 from a table as 0.7 and did not allow it to change. The other two parameters were allowed to change.

(c) The energy E_0 needed to excite the electron from the inner shell to the Fermi level is not known theoretically. Thus, it is necessary to vary this parameter within the fitting program. This is achieved by providing the fitting program with the experimental EXAFS spectrum as a function of energy and converting it into a function of the photoelectron wave number within the fit routine with a variable E_0.

(d) The **k**-independent phase shift θ discussed in Sec. III was also allowed to vary. On the other hand, the phase shifts which are proportional to k^{-1} were not needed in this case. The reason is that this system has only one type of atom, Cu, and changing E_0 within a small range is equivalent to changing a phase proportional to k^{-1}.

In conclusion, the parameters that were allowed to vary are E_0, θ, λ, and one mean-squared displacement σ^2 for each of the first three shells. The mean-squared displacement of the fourth was taken equal to that of the third.

As mentioned before, the actual fitting of theory and experiment was done in **r** space. In transforming the spectrum from **k** space to **r** space, we multiply both theoretical and experimental spectra by a function that tends to increase the spectrum at large **k** so as to obtain a better separation of the shells in **r** space. In addition, we round off the edges of the spectrum to avoid ringing. It should be emphasized that since all we are concerned with here is obtaining a fit between theory and experiment over a broad range in both **k** and **r**, the separation of the shells is much less critical than in the ordinary data analysis. We can therefore afford to multiply the spectrum by k^{ν}, where ν is small, about 1, so as not to give the high **k** part of the spectrum too large a weight, in view of the fact that the signal-to-noise ratio in this range is not as good as at small **k**.

We found that it is easier to fit the first shell first, because it is well separated from the others. This provides the values for E_0, θ, λ, and σ_1^2. To fit the other three shells, all that was necessary was to introduce the other two mean-squared displacements σ_2^2 and σ_3^2. In fitting all the parameters the first four changed relatively little from the values obtained by fitting to the first shell. The best fit was obtained with the following values: E_0 is 3 eV below the midpoint of the main rise at the absorption edge; $\theta=-1.19$ rad; $\lambda=5.7$ Å; $\sigma_1^2=5.7\times10^{-3}$ Å^2; $\sigma_2^2=6.1\times10^{-3}$ Å^2; $\sigma_3^2=11.6\times10^{-3}$ Å^2. It should be emphasized that E_0 and θ are varied in order to account for flaws in the theory. Thus their fit values are at present not physically significant. The mean free path λ and the mean-squared displacements σ^2 are significant, but should be treated with caution. Their values can be compared with the experimentally[27] derived ones of $\lambda=7.4$ Å, $\sigma_1^2=7.7\times10^{-3}$ Å^2, $\sigma_2^2=10.6\times10^{-3}$ Å^2, and $\sigma_3^2=9.87\times10^{-3}$ Å^2.

The fit results can be seen in Figs. 2–4. Figures 2 and 3 show the fit of the Fourier transform and its absolute value, respectively. The vertical lines represent the range in which the fit was performed. Notice that in this range the fit is good except for a small range near 3.6 Å in the imaginary part and near 3.8 Å in the real part. These discrepancies show up in Fig. 3—the absolute value of the Fourier transform—at the minimum near 3.6 Å. Comparing the discrepancies with the noise as seen at large distances suggests that the misfits are within the noise level. In Fig. 4 the experimental curve is the back Fourier transform of the spectrum in the fitting range. Comparison of theory and experiment shows only small misfits. This fit was performed over a range of 8.5 Å^{-1} in Δk and 3.8 Å in Δr. According to Eq. (9) this corresponds to 20 independent experimental points, which is much larger than the six variable parameters allowed to vary in the fit.

We now compare the various multiple-scattering contributions. Figure 5 shows a comparison among the different contributions to the EXAFS from single scattering, noncollinear double scattering, and collinear double and triple scattering. Indeed, as expected, only single-scattering contributions are important for the first shell. But, in the region of higher shells the multiple-scattering contributions are very important. This can also be seen clearly in the comparison of the absolute values of these contributions shown in Fig. 6. In particular, the noncollinear double scattering is important above 3 Å as predicted in Ref. 18. This is important to note, since it is common practice to neglect this contribution. In Fig. 7 we show a comparison of the single-, double-, and triple-scattering contributions involving the center atom and two additional Cu atoms along the face diagonal. Notice

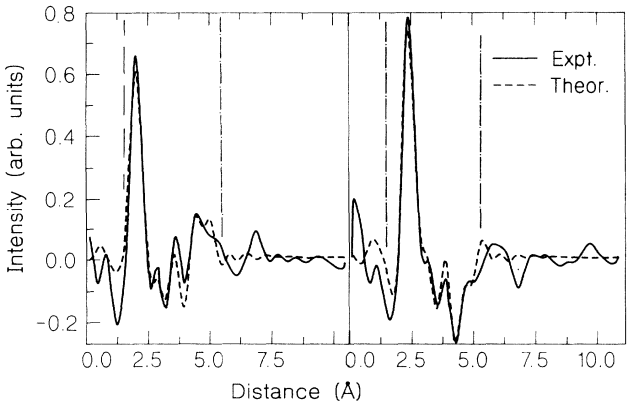

FIG. 2. The real (right) and imaginary (left) parts of the Fourier transform of the EXAFS spectra of copper. The vertical lines show the fitting range.

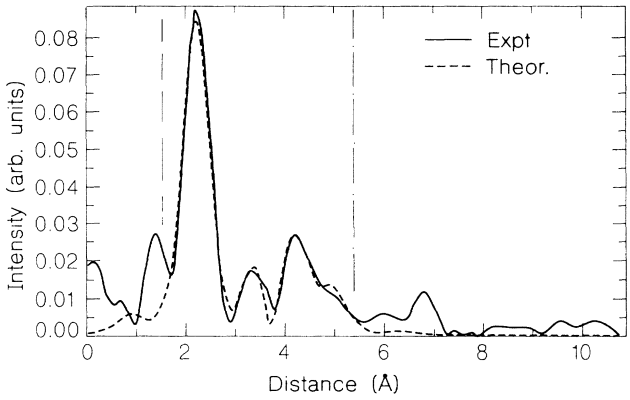

FIG. 3. The absolute value of the Fourier transform of the EXAFS spectrum of copper. Experimental, solid line; theoretical, dashed line. The vertical lines show the fitting range.

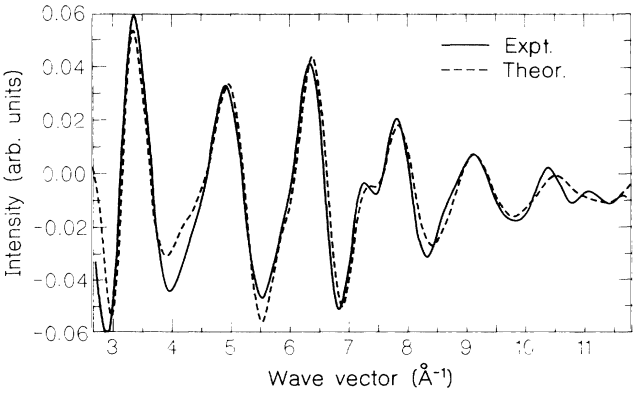

FIG. 4. The EXAFS spectra of copper as a function of the photoelectron wave number. The experimental spectrum has been filtered to contain only the part between the vertical lines in Fig. 3.

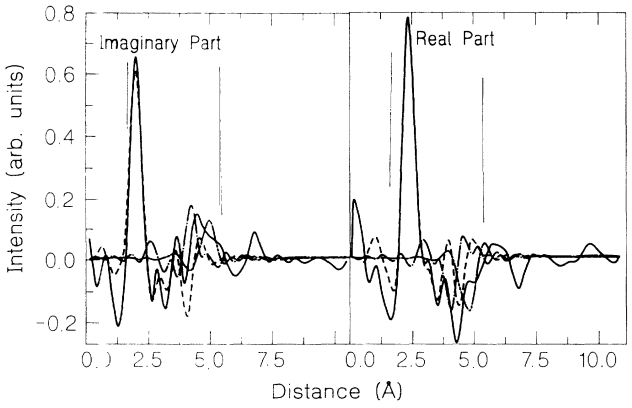

FIG. 5. The theoretical contributions of different scattering configurations of the photoelectron to the EXAFS of copper: (a) real part, (b) imaginary part. Experimental, solid line; single scattering, dashed line; noncollinear double scattering, dash-dotted line; collinear double and triple scattering, dash-double-dotted line.

that both double- and triple-scattering contributions are much larger than the single-scattering contribution. This is typical when the atoms are collinear, as has been well documented previously, both experimentally[28,29] and theoretically.[3] However, the enhancement of the multiple scattering over simple scattering is not as large as the plane-wave approximation estimates.[30] The curved-wave calculation as utilized here does account correctly for the enhancement, in agreement with previous work.[31,32]

Since the noncollinear double-scattering contribution is usually ignored, it is useful to discuss why it is important here. The noncollinear double-scattering contribution of a single path is indeed small, but due to the large multiplicity of these paths their total contribution is about as large as the single-scattering contributions from the second and third shells. In agreement with a previous es-

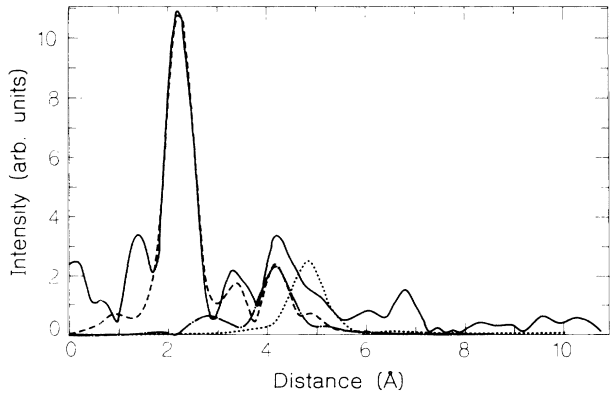

FIG. 6. Absolute values of the Fourier transform of the various multiple-scattering contributions to the EXAFS spectrum of copper. Experimental, solid line; single scattering, dash line; noncollinear double scattering, dashed-dotted line; collinear double and triple scattering, dotted line.

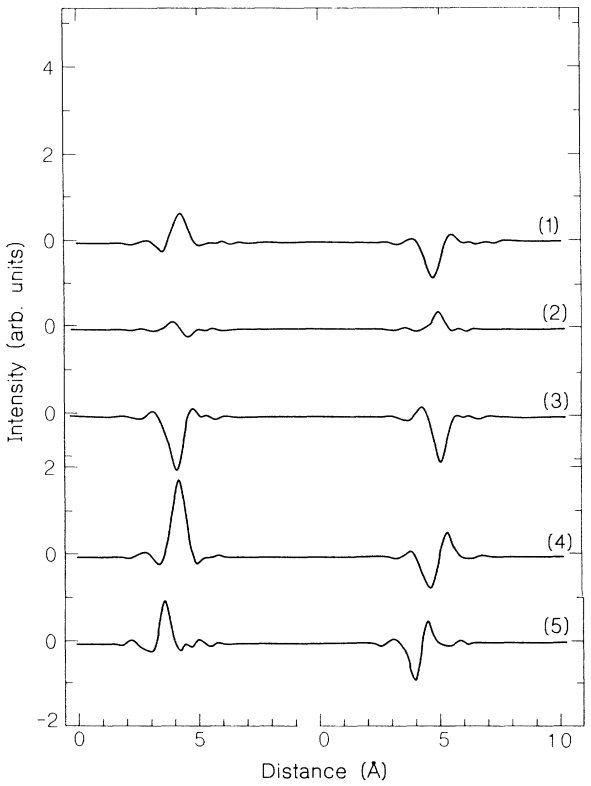

FIG. 7. Comparison among the various components of the real (right) and the imaginary (left) parts of the Fourier transform of the fourth shell and the noncollinear scattering contributions. (1), Total fourth-shell contribution including single-, double-, and triple-scattering contributions; (2), fourth-shell single scattering; (3), fourth-shell collinear double scattering; (4), fourth-shell collinear triple scattering; (5), total double noncollinear scattering.

timate,[18] the main noncollinear double-scattering contribution arises from paths that are equivalent to the path involving the center atom and the atoms at [110] and [121]. There are 48 such paths and their total contribution is also shown in Fig. 7. The large size of this contribution is a result of the fact that the bond angle in this configuration is only 60°, deviating significantly from 90°. In fact, it was pointed out previously[8,18] that if the bond angle ϕ is 90°, the multiple-scattering contribution will be essentially zero because of a $\cos\phi$ dependence in the multiple-scattering contribution for K-shell excitations.

V. SUMMARY AND CONCLUSIONS

The EXAFS data analysis method described here has several important advantages. The theoretical calculation of the EXAFS spectrum takes into account the curved-wave nature of the wave function and calculates exactly both single- and double-scattering contributions within the limitations of the calculated $X\alpha$ potential. The triple scattering is evaluated using the Rehr *et al.*[11] approximation, which is exact for collinear scattering and deviates only a little from the right value at close to collinear scattering conditions. The theoretical calculations have limitations, however, and to compensate for these limitations we use a number of variable parameters that are refined together with the structural parameters of interest in order to obtain a good fit with experiment. This combination can accurately represent the experimental spectra up to fourth-neighbor distances. The test case discussed here, as well as five other systems that were analyzed using this method, shows that the parameters we chose are adequate in order to compensate for the flaws of the theory and render a very good fit with experiment. These systems, which belong to the perovskite family, are $KTaO_3$, $NaTaO_3$, $KTaO_3$:Nb, ReO_3, and the high-T_c superconducting material $YBa_2Cu_3O_7$. The results will be discussed in detail elsewhere.

The fitting method presented here has several advantages. The amplitude and phase functions of each configuration and their derivatives are calculated only once. This eliminates the need to calculate them many times within the fitting process. Moreover, they can be used for various structures that differ slightly from each other. Thus, EXAFS data, measured at different temperatures or at different structural phases, can be analyzed using the same amplitude and phase functions. The analysis is carried out in the distance representation, which allows us to limit the order of the multiple scattering that affects the results.

The analysis of the Cu EXAFS spectrum clearly shows that, above the first shell, multiple-scattering contributions cannot be neglected and may in certain cases even be dominant. As is well known, collinear double and triple scattering are as large as or even larger than the corresponding single-scattering contributions. However, even noncollinear double scattering is found to be as large as some single-scattering contributions. The main noncollinear contributions are due to configurations with a large number of equivalent paths and a bond angle significantly smaller than 90°.

In conclusion, we present evidence that the EXAFS analysis method presented here is quite generally applicable and can be relatively easily implemented using a fast microcomputer. We believe that the introduction of this or similar analysis methods will result in an important improvement in the quality of the information obtained from EXAFS.

ACKNOWLEDGMENTS

It is a pleasure to acknowledge the support of the United States–Israel Binational Science Foundation (Jerusalem, Israel) under Contract No. 84-00257, and the U.S. Department of Energy under Contract No. DE-FG06-84ER45163.

*Present address: Electronics Division, Los Alamos National Laboratory, Los Alamos, NM 87545.
†Permanent address: Department of Physics (FM-15), University of Washington, Seattle, WA 98195.

[1]D. E. Sayers, E. A. Stern, and F. Lytle, Phys. Rev. Lett. **27**, 1204 (1971).
[2]W. L. Schaich, Phys. Rev. B **8**, 4028 (1973).
[3]P. A. Lee and J. B. Pendry, Phys. Rev. B **11**, 2795 (1975).
[4]C. A. Ashley and S. Doniach, Phys. Rev. B **11**, 1279 (1975).
[5]P. J. Durham, J. B. Pendry, and C. H. Hodges, Comput. Phys. Commun. **25**, 193 (1982).
[6]S. J. Gurman and R. F. Pettifer, Philos. Mag. B **40**, 345 (1979).
[7]E. A. Stern and S. M. Heald, in *Handbook on Synchrotron Radiation,* edited by E. E. Koch (North-Holland, New York, 1983), Vol., 1, p. 986.
[8]G. Bunker and E. A. Stern, Phys. Rev. Lett. **52**, 1990 (1984).
[9]D. D. Vvedensky, D. K. Saldin, and J. B. Pendry, Comput. Phys. Commun. **40**, 42 (1986).
[10]J. E. Müller and W. L. Schaich, Phys. Rev. B **27**, 6489 (1983).
[11]J. J. Rehr, R. C. Albers C. R. Natoli, and E. A. Stern, Phys. Rev. B **34**, 4350 (1986); J. J. Rehr and R. C. Albers, *ibid.* **41**, 8139 (1990).
[12]R. C. Albers, A. K. McMahan, and J. E. Müller, Phys. Rev. B **31**, 3435 (1985).
[13]S. J. Gurman, N. Binsted, and I. Ross, J. Phys. C **17**, 143 (1984).
[14]L. F. Mattheiss, J. H. Wood, and A. C. Switendick, in *Methods in Computational Physics,* edited by B. Adler, S. Fernback, and M. Rotenberg (Academic, New York, 1968), Vol. 8, p. 63.
[15]S. J. Gurman, J. Phys. C **21**, 3699 (1988).
[16]J. E. Harris, D. W. L. Hukins, and S. S. Hasnain, J. Phys. C **19**, 6859 (1986).
[17]R. W. Strange, N. J. Blackburn, P. F. Knowles, and S. S. Hasnain, J. Am. Chem. Soc. **109**, 7157 (1987).
[18]E. A. Stern, in *X-Ray Absorption Principles, Applications, Techniques of EXAFS, SEXAFS, XANES,* edited by D. C. Konigsberger and R. Prins (Wiley, New York, 1988), Chap. 1, pp. 34–36.
[19]G. Descleaux, J. Phys. B **4**, 631 (1971); Comput. Phys. Commun. **9**, 31 (1975).
[20]P. A. Lee and G. Beni, Phys. Rev. B **15**, 2862 (1977).
[21]J. Mustre de Leon, Ph.D. thesis, University of Washington, 1989.
[22]S. H. Chou, J. J. Rehr, E. A. Stern, and E. R. Davidson, Phys. Rev. B **35**, 2604 (1986).
[23]B. K. Teo and P. A. Lee, J. Am. Chem. Soc. **101**, 2815 (1979).
[24]D. M. Brink and G. R. Satchler, *Angular Momentum* (Oxford University Press, Oxford, 1968).
[25]P. A. Lee, P. H. Citrin, P. Eisenberger, and B. M. Kincaid, Rev. Mod. Phys. **53**, 769 (1981).
[26]Y. Yacoby, M. Brettschneider, and M. Bezalel, Rev. Sci. Instrum. **58**, 588 (1987).
[27]J. J. Rehr, E. A. Stern, R. L. Martin, and E. R. Davidson, Phys. Rev. B **17**, 560 (1978).
[28]E. A. Stern, B. Bunker, and S. M. Heald, Phys. Rev. B **21**, 5521 (1980).
[29]E. A. Stern, D. E. Sayers, and F. W. Lytle, Phys. Rev. B **11**, 5836 (1975).
[30]B. K. Teo, J. Am. Chem. Soc. **103**, 3990 (1981).
[31]J. J. Rehr, R. Albers, J. Mustre de Leon, and E. A. Stern (unpublished).
[32]R. V. Vedrinskii and L. A. Bugaev, J. (Paris) Phys. Colloq. **47**, C8-C9 (1986).